This is a preprint, the final version is subject to change, of the American Mineralogist (MSA)
Cite as Authors (Year) Title. American Mineralogist, in press.
DOI: https://doi.org/10.2138/am-2019-6750

Revision 3

Stability, Composition, and Crystal Structure of Fe-bearing Phase E in the Transition Zone

Li Zhang[1,2,3*], Joseph R. Smyth[2], Takaaki Kawazoe[4], Steven D. Jacobsen[5], Jingjing Niu[3], Xuejing He[3], Shan Qin[3]

[1] School of Earth Science and Resources, China University of Geosciences, Beijing 100083, China.

[2] Department of Geological Sciences, University of Colorado, Boulder, CO 80309, U.S.A.

[3] School of Earth and Space Sciences, Peking University, Beijing, 100871, China.

[4] Department of Earth and Planetary Systems Science, Hiroshima University, Higashi-Hiroshima 739-8526, Japan.

[5] Department of Earth and Planetary Sciences, Northwestern University, Evanston, Illinois 60208, U.S.A.

ABSTRACT

Fe-bearing phase E coexisting with ringwoodite and wadsleyite has been synthesized at near-geotherm temperatures in hydrous KLB-1 peridotite compositions held at 18 and 19 GPa, and 1400 ºC for 27 hours. The long heating duration time of syntheses implies

that phase E can be a stable component of the mantle under hydrous conditions. Single-crystal X-ray diffraction analyses show that the M1 octahedral site is 72.1-75.2 at% occupied, whereas the M2 and tetrahedral Si sites are 2.4-2.9 at% and 18.9-19.8 at% occupied respectively. The M1 site occupancies show a positive correlation with Fe/Mg molar ratios, indicating that Fe mainly occupies the M1 site in the phase E structure. High-pressure Raman spectroscopy shows that the framework Raman frequencies of Fe-bearing phase E increase continuously with increasing pressures up to 19 GPa at room temperature and there is no indication for a major change in the crystal structure. If transition-zone regions adjacent to subducting slabs are hydrated by fluids generated at the top of the lower mantle, Fe-bearing phase E is expected to occur at wadsleyite-ringwoodite phase transition boundary (about 520 km) as an important phase for incorporating water.

Keywords : phase E, transition zone, X-ray diffraction, high-pressure Raman spectroscopy

INTRODUCTION

Phase E is one of the dense hydrous magnesium silicates (DHMS) that may play a significant role in the global hydrogen cycle as water carriers in subducting slabs (e.g., Ohtani et al. 2004). Phase E was discovered by high-pressure phase relation studies in the system Mg_2SiO_4 + 20 wt% H_2O (Kanzaki 1991). Previous studies demonstrated that

phase E can contain up to 18 wt.% H_2O and can occur at depth of 350 km to about 500 km within subduction-zone environments (e.g., Frost 1999; Shieh et al. 2000). In addition, a possible natural phase E was observed in olivine from kimberlitic nodules as nanometer-sized inclusions (Khisina and Wirth 1997).

As a consequence of unit-cell-scale disorder, phase E has broad compositional and density variations (Kanzaki et al. 1992; Kudoh et al. 1993). In the MgO-SiO_2-H_2O system, phase E is stable along subduction geotherms through the base of the upper mantle and the top of the transition zone (e.g., Iwamori, 2004). Frost and Fei (1998) showed that phase E can coexist with super-hydrous phase B at 17.5 GPa and 1100 ºC. In the CaO-MgO-Al_2O_3-SiO_2-H_2O pyrolite system, phase E was observed at 12 GPa and 1050 ºC coexisting with hydrous wadsleyite (Litasov and Ohtani 2003). Kawamoto (2004) reported the stabilities of hydrous phases in water bearing (13.6 wt.% H_2O) CaO-MgO-FeO-Al_2O_3-TiO_2-SiO_2 system, showing that Fe-bearing phase E can coexist with wadsleyite, stishovite and garnet at 17 GPa and 1000 ºC. Kawamoto et al. (1995) determined the stability field of phase E in H_2O-saturated KLB-1 peridotite (CaO-MgO-FeO-Al_2O_3-TiO_2-SiO_2-H_2O system) at 6 to 15 GPa, indicating that Fe-bearing phase E can coexist with wadsleyite, garnet, and enstatite at mantle geotherm (15.5 GPa and 1400 ˚C).

Phase E has a unique cation-disordered crystal structure (Figure 1), which has been

solved and refined in space group $R\bar{3}m$ (e.g., Kudoh et al. 1993). The structure contains layers stacked in a rhombohedral arrangement with brucite-type units. The layers are cross linked by Si in tetrahedral coordination, Mg in octahedral coordination, as well as hydrogen bonds (e.g., Kanzaki et al. 1992; Kudoh et al. 1993; Tomioka et al. 2016). Single-crystal X-ray diffraction analyses indicated that the interlayer octahedra (M2 site) and tetrahedra (Si site) are only about 1-2 and 19-20 at% occupied respectively. To avoid sharing faces with interlayer tetrahedra, there are also vacancies (up to 34 at%) within the intralayer octahedra (M1 site) (Kudoh et al. 1993; Uchiyama et al. 2011). High-pressure Raman spectroscopy of pure-Mg phase E indicated that all framework modes shift continuously with increasing pressures to 19 GPa and there is no indication for a phase transition or amorphization of the structure (Kleppe et al. 2001). For high-pressure infrared spectroscopy, according to Shieh et al (2009), no structural phase transition or amorphization was found for pure-Mg phase E to pressures up to 40 GPa.

To better understand the stability, composition, and crystal structure of Fe-bearing phase E, high-pressure sample syntheses, electron microprobe analyses, single-crystal X-ray diffraction analyses, and high-pressure Raman spectroscopy were conducted in this study.

EXPERIMENTAL METHODS

Phase E and coexisting phases were synthesized in a 1200 tonne Sumitomo multi-anvil press at Bayerisches Geoinstitut, University of Bayreuth, Germany at 18 GPa

(run SS1603) and at 19 GPa (run SS1601), at 1400 ºC with 27-hour heating, using 10/5 assemblies which can be employed to generate sample pressures up to 21 GPa. Pressure calibration of 10/5 assembly was based on phase transitions in Bi, ZnS and GaAs at room temperature and coesite-stishovite, α-β Mg_2SiO_4, and β-γ Mg_2SiO_4 equilibria at high temperature (1200-1600 ºC). The uncertainties in pressure calibrations were estimated to be less than 0.5 GPa (Rubie 1999). We used a KLB-1 peridotite composition as starting material which was mixed from oxides of SiO_2 (44.84 wt.%), MgO (27.66 wt.%), FeO (8.20 wt.%), Al_2O_3 (3.51 wt.%) and CaO (3.07 wt.%), plus 3.50 wt.% water (H_2O) as $Mg(OH)_2$ (11.80 wt.%). KLB-1 composition is considered to be similar to pyrolite suggested by Ringwood (1975) (e.g., Takahashi 1986). The compositions of the run products (Figure 2) were analyzed with the electron microprobe (JEOL 8900) with a 15-kV accelerating voltage, 5 nA beam current, 5 μm probe diameter, using natural or synthetic standards.

Raman spectra and fluorescence background (Figures 3, 4, and 5) were collected with a Renishaw inVia reflex laser Raman spectrometer (with a spectral resolution of 1 cm^{-1} and a focal length of 250 mm), using a liquid N_2 cooled CCD detector. The spectra were excited by a 532 nm diode-pumped solid-state laser (2400 gr/mm grating was used) focused down to a spot of ~ 1 μm in diameter on sample. All bands were collected from randomly oriented specimens using two accumulations with 10 s exposure time. 50× and 20× microscope objectives were employed at ambient conditions and at conditions of

high-pressure, respectively.

For high-pressure Raman spectroscopy, one optically transparent, inclusion-free phase E crystal with flat surfaces measuring ~ 100×50×50 μm in size was selected and mounted in a symmetric-type diamond-anvil cell. Two ruby spheres were loaded next to the phase E crystal for pressure calibration (e.g., Mao et al. 1986), using culets of ~ 0.4 mm in diameter. A rhenium (Re) gasket was pre-indented to a thickness of ~ 60 μm with a ~ 0.2 mm diameter hole as the sample chamber. Fluid argon (Ar) was loaded as a pressure-transmitting medium at 300 MPa according to the loading technique reported by Rivers et al. (2008). Although the hydrostatic limit of argon is about 10 GPa, the estimated pressure gradients are lower than 0.2 GPa at pressures up to 19 GPa (Klotz et al. 2009). Unpolarized Raman spectra were collected to 19 GPa in the range of 300 cm^{-1} to 1200 cm^{-1}.

Two phase E samples (samples 1 and 2) from the synthesis runs were chosen and mounted on glass fibers and centered on a four-circle diffractometer for single-crystal X-ray diffraction analysis. Intensity data were collected with a Bruker APEX II CCD detector on a Siemens/MAC-Science 18 kW rotating Mo-anode X-ray generator at the University of Colorado, Boulder, using 50 kV voltage, 250 mA current and calibrated radiation (λ = 0.71073 Å). Crystal structures were refined from the intensity data sets using SHELXL-2018 in the package WINGX (e.g., Sheldrick 2018). Only Mg was modeled in the octahedral sites. CIF is available as a deposit item. Precession images for

axial crystallographic directions (0kl, h0l, and hk0) are shown in Appendix Figure 1.

RESULTS

According to the phase compositions shown in (Table 1), in run SS1601, phase E coexists with ringwoodite, garnet, and minor amounts of phase δ-H at about 19 GPa and 1400 ºC. In run SS1603, phase E coexists with wadsleyite, garnet, clinopyroxene, and minor amounts of phase δ-H at about 18 GPa and 1400 ºC. The compositional differences of the products between two synthesis runs are mainly due to wadsleyite-ringwoodite phase transition (e.g., Ringwood and Major 1966) and pyroxene-garnet transformation (e.g., Ringwood 1967). The electron microprobe analyses show that phase E contains 4.5-6.2 wt.% FeO and about 1.4 wt.% Al_2O_3 (Table 1). If deficits in weight are ascribed to H_2O, the formula units of phase E samples (SS1601 and SS1603) are estimated to be $Mg_{2.08}Fe_{0.17}Al_{0.06}Si_{1.23}O_6H_{2.42}$ and $Mg_{2.14}Fe_{0.12}Al_{0.05}Si_{1.20}O_6H_{2.50}$, respectively.

As shown in Figures 3, at ambient conditions, the fluorescence bands of Fe-bearing phase E are consistent with those of pure-Mg phase E (Kleppe et al. 2001). As shown in Figure 4a, for two Fe-bearing phase E samples (from run products of SS1601 and SS1603, respectively) in this study, the Raman spectra show two broad bands at about 690 cm^{-1} and 900 cm^{-1}. For pure-Mg phase E reported by Kleppe et al. (2001), two bands at similar positions (at about 690 cm^{-1} and 950 cm^{-1}) can also be observed (Figure 4a). Liu et al. (1997) reported two sharp Raman bands of pure-Mg phase E at ambient conditions at 817 cm^{-1} and 850 cm^{-1}. However, their sample may have been mixed with an impurity phase

(e.g., Kleppe et al. 2001). In the OH-stretching region (3000 - 3800 cm^{-1}), two broad bands at about 3450 cm^{-1} and 3580 cm^{-1} are observed, indicating hydroxyl groups in the crystal structure (Figure 4a). In the range from 1200 cm^{-1} to 3000 cm^{-1}, a weak band occurs at 2500 - 2650 cm^{-1} in the Raman spectra of both pure-Mg phase E (Kleppe et al. 2001) and Fe-bearing phase E (this study). This band also indicates the presence of hydrogen bonded hydroxyl groups (Kleppe et al. 2001). The relative intensities of all Raman bands between 100 cm^{-1} and 3800 cm^{-1} change with varying orientation of the phase E crystal relative to the incident laser beam. As a result, the weak band in the region between 1200 cm^{-1} and 3000 cm^{-1} can-not be observed in some Raman spectra of phase E (Figure 4a). The Raman spectrum of the wadsleyite which coexists with phase E shows two board bands at about 3376 cm^{-1} and 3580 cm^{-1}, indicating that the wadsleyite is also hydrous. For the ringwoodite which coexists with phase E, Raman bands correspond to stretching vibrations of hydroxyl can-not be observed (Figure 4b). According to the high-pressure Raman spectroscopy in this study, the framework Raman frequencies of Fe-bearing phase E increase continuously with increasing pressures over the investigated pressure range (Figure 5).

As previously observed in pure-Mg phase E (Kudoh et al. 1993), the Fe-bearing phase E in this study is also significantly disordered. According to single-crystal X-ray diffraction analyses (Table 2), the M1 site in octahedral coordination is about 72.1-75.2 at% occupied, whereas the M2 site is about 2.4-2.9 at% occupied. As shown in Table 2 the

bond distances of M1-O are 2.0764(17) Å and 2.0702(12) Å for sample 1 and sample 2, respectively. The bond distances of M2-O are 2.0690(17) Å and 2.0609(12) Å for sample 1 and sample 2, respectively. Compared to M1-O, M2-O distances are shorter. The four-coordinated Si forms a distorted tetrahedron with O. This tetrahedron has one typical Si-O distance of 1.666(3)-1.670(6) Å and three long distance of 1.824(1)-1.832(2) Å. The Si site occupancies were estimated to be 18.9-19.8 at% for two phase E samples (Table 2).

DISCUSSION

Previously reported pure-Mg phase E is only stable at subduction zone geotherms (e.g., Frost and Fei 1998). For Fe-bearing phase E, Kawamoto et al. (1995) demonstrated that it can also be stable at mantle geotherm (15.5 GPa and 1400 ºC). The results of sample syntheses in this study indicate that Fe-bearing phase E can occur at higher pressures and near-geotherm temperature (18-19 GPa and 1400 ºC). The long heating duration time (27 h) implies that it is a stable component of KLB-1 + 3.5 wt.% H_2O. For the coexisting phases in the run products (Figure 2), wadsleyite, ringwoodite, clinopyroxene, and garnet are all constituent mineral phases in the transition zone (e.g., Ringwood 1958; Ringwood 1967; Ringwood and Major 1967). In addition, the minor coexisting phase δ-H is also expected to be stable in the transition zone and the lower mantle at geotherm temperatures under hydrous conditions (e.g., Duan et al. 2018; Ohira et al. 2014; Ohtani 2015).

Previous studies showed that water stored in hydrous ringwoodite and super-hydrous phase B can dehydrate at the top of the lower mantle in stagnant subducted slabs (e.g., Litasov and Ohtani 2007; Ohtani et al. 2003). As a result, the overlying transition-zone regions can be saturated by the ascending fluids generated in the dehydration processes (e.g., Litasov and Ohtani 2007; Ohtani et al. 2003). Therefore, Fe-bearing phase E is expected to occur near the wadsleyite-ringwoodite boundary (about 520 km) in these hydrated regions.

At ambient conditions, the stretching vibration of the SiO_4 tetrahedra may result in the occurrence of the modes between 690 cm^{-1} and 960 cm^{-1} for Raman spectra of phase E and other silicates (Kleppe et al. 2001). Therefore, in this study, we attribute the bands at about 690 cm^{-1} and 900 cm^{-1} (Figure 4a) to the SiO_4 tetrahedra in the crystal structure of Fe-bearing phase E (SS1601 and SS1603). The broadness of these bands is likely due to the cation disorder. The site disorder results in local structural distortions leading to distributions of Si-O, Mg-O, and O-O bond lengths and bond strengths that are in turn reflected in the broader Raman bands (Kleppe et al. 2001).

For Fe-bearing phase E, high-pressure Raman spectroscopy in this study shows that all bands observed from 300 cm^{-1} to 1200 cm^{-1} shift continuously with pressures over the investigated pressure range (up to 19 GPa) without significant broadening and without decreasing intensities, indicating that Fe-bearing phase E does not appear to undergo any structural transitions at room temperature up to at least 19 GPa (Figure 5). This

observation is consistent with the Raman spectroscopy results for pure-Mg phase E to 19 GPa (Kleppe et al. 2001).

Single-crystal X-ray diffraction analyses in this study also indicate a cation-disordered phase E structure. As shown in Table 2, the M2 and Si sites in the Fe-bearing phase E are significantly vacant. For these two sites, the estimated site occupancies (2.4-2.9 at% and 18.9-19.8 at%) are in accordance with those in pure-Mg phase E (Kudoh et al. 1993). However, the M1 site has relatively higher occupancies (72.1-75.2 at%) than that in pure-Mg phase E (66.4-68.7 at%; Kudoh et al. 1993). The positive correlation between M1 site occupancies and Fe/Mg molar ratios (Figure 6) indicates that Fe mainly occupies the M1 site in the phase E structure. In order to avoid sharing faces with tetrahedra in the Si site, the associated octahedra in the M1 site must be vacant (Kudoh et al. 1993). Therefore, the shortened Si-O distances of the distorted Si tetrahedra (Table 2) are due to the relaxation of the basal oxygen atom positions caused by the absence of Mg.

IMPLICATIONS

First, Fe-bearing phase E can occur in the mantle transition zone at near-geotherm temperature (18-19 GPa and 1400 °C) under hydrous conditions. The long heating duration time (27 h) of sample syntheses implies that it can be a stable component in the system KLB-1 plus 3.5 wt.% H_2O. Therefore, Fe-bearing phase E is expected to occur near the wadsleyite-ringwoodite boundary (about 520 km) in the hydrated regions.

Second, the M1 site occupancies measured by X-ray diffraction show a positive correlation with Fe/Mg molar ratios, indicating that Fe mainly occupies the M1 site in the phase E structure. The high-pressure Raman spectroscopy indicates that Fe-bearing phase E does not appear to undergo any structural transitions at room temperature up to at least 19 GPa.

ACKNOWLEDGEMENTS

This study was supported by the National Natural Science Foundation of China (No. 41802035) and U.S. National Science Foundation (Grant EAR 11-13369 and EAR 14-16979 to J.R.S.) and China Postdoctoral Science Foundation (No. 2017M620508). Multi-anvil experiments were supported by Bayerisches Geoinstitut Visitors Program. L.Z. acknowledges support from Peking University Boya Postdoctoral Fellowship. S.D.J acknowledges support from U.S. National Science Foundation Grant EAR-1452344, the Carnegie/DOE Alliance Center, the David and Lucile Packard Foundation, and the Alexander von Humboldt Foundation.

REFERENCES

Duan, Y., Sun, N., Wang, S., Li, X., Guo, X., Ni, H., Prapapenka, V. B., and Mao, Z. * (2018) Phase stability and thermal equation of state of δ-AlOOH: Implication for water transportation to the deep lower mantle. Earth and Planetary Science letters, 494, 92-98.

Frost, D.J. (1999) The stability of dense hydrous magnesium silicates in Earth's transition

zone and lower mantle, in Fei, Y., Bertka, C.M., and Mysen B.O., eds., Mantle Petrology: Field Observations and High Pressure Experimentation: A Tribute to F.R. Boyd. Geochemical Society Special Publication, 6, 283–296.

Frost, D. J., and Fei, Y. W. (1998) Stability of phase D at high pressure and high temperature. Journal of Geophysical Research-Solid Earth, 103, B4, 7463-7474.

Iwamori, H. (2004) Phase relations of peridotites under H_2O-saturated conditions and ability of subducting plates for transportation of H_2O. Earth and Planetary Science Letters, 227, 1-2, 57-71.

Kanzaki, M. (1991) Stability of Hydrous Magnesium Silicates in the Mantle Transition Zone. Physics of the Earth and Planetary Interiors, 66, 3-4, 307-312.

Kanzaki, M., Stebbins, J., and Xue, X. (1992) Characterization of crystalline and amorphous silicates quenched from high-pressure by 29 Si MAS NMR spectroscopy. High-Pressure Research: Application to Earth and Planetary Sciences, 89–100. American Geophysical Union.

Kawamoto, T. (2004) Hydrous phase stability and partial melt chemistry in H_2O-saturated KLB-1 peridotite up to the uppermost lower mantle conditions. Physics of the Earth and Planetary Interiors, 143, 387-395.

Kawamoto, T., Leinenweber, K., Herving, R.L., and Holloway, J.R. (1995) Stability of hydrous minerals in H_2O-saturated KLB-1 peridotite up to 15 GPa, in Farley, K.A., ed., Volatiles in the Earth and Solar System: Melville, New York, American Institute

of Physics Conference Proceeding, 341, 229–239.

Kawamoto, T., Matsukage, K. N., Mibe, K., Isshiki, M., Nishimura, K., Ishimatsu, N., and Ono, S. (2004) Mg/Si ratios of aqueous fluids coexisting with forsterite and enstatite based on the phase relations in the Mg_2SiO_4-SiO_2-H_2O system: American Mineralogist, 89, 10, 1433-1437.

Khisina, N.R. and Wirth, R. (1997) Water-bearing inclusions in olivine from kimberlite: High-pressure hydrous silicates? EOS, 78, 735.

Kleppe, A. K., Jephcoat, A. P., and Ross, N. L. (2001) Raman spectroscopic studies of phase E to 19 GPa. American Mineralogist, 86, 10, 1275-1281.

Klotz, S., Chervin, J.C., Munsch, P., and Le Marchand, G. (2009) Hydrostatic limits of 11 pressure transmitting media. Journal of Physics D-Applied Physics, 42(7).

Kudoh, Y., Finger, L. W., Hazen, R. M., Prewitt, C. T., Kanzaki, M., and Veblen, D. R. (1993) Phase E - a High-pressure hydrous silicate with unique crystal-chemistry. Physics and Chemistry of Minerals, 19, 6, 357-360.

Litasov, K., and Ohtani, E. (2003) Stability of various hydrous phases in CMAS pyrolite-H_2O system up to 25 GPa. Physics and Chemistry of Minerals, 30, 3, 147-156.

Litasov, K.D., Ohtani, E. (2007) Effect of water on the phase relations in Earth's mantle and deep water cycle. Special Paper of the Geological Society of America, 421, 115–156.

Liu, L.G., Mernagh, T.P., Lin, C.C., and Irifune, T. (1997) Raman spectra of phase E at various pressures and temperatures with geophysical implications. Earth and Planetary Science Letters, 149(1-4), 57-65.

Mao, H.K., Xu, J., Bell, P.M. (1986) Calibration of the Ruby Pressure Gauge to 800-Kbar under Quasi-Hydrostatic Conditions. Journal of Geophysical Research-Solid Earth and Planets, 91(B5), 4673-4676.

Ohira, I., Ohtani, E., Sakai, T., Miyahara, M., Hirao, N., Ohishi, Y., and Nishijima, M. (2014) Stability of a hydrous δ-phase, AlOOH–$MgSiO_2(OH)_2$, and a mechanism for water transport into the base of lower mantle. Earth and Planetary Science Letters, 401, 12-17.

Ohtani, E. (2015) Hydrous minerals and the storage of water in the deep mantle. Chemical Geology, 418, 6-15.

Ohtani, E., Litasov, K., Hosoya, T., Kubo, T., and Kondo, T. (2004) Water transport into the deep mantle and formation of a hydrous transition zone. Physics of the Earth and Planetary Interiors, 143, 255-269.

Ohtani, E., Toma, M., Kubo, T., Kondo, T., and Kikegawa, T. (2003) In situ X-ray observation of decomposition of superhydrous phase B at high pressure and temperature. Geophysical Research Letters, 30, 2.

Ringwood, A.E. (1958) The constitution of the mantle. 1: Thermodynamics of the olivine-spinel transition. Geochimica Et Cosmochimica Acta, 13, 4, 303-321.

Ringwood, A.E. (1967) Pyroxene-garnet transformation in Earth's Mantle. Earth and Planetary Science Letters, 2, 3, 255-263.

Ringwood, A.E. (1975) Composition and petrology of the Earth's mantle (McGraw Hill, New York), p. 618.

Ringwood, A.E., and Major, A. (1966) Synthesis of Mg_2SiO_4-Fe_2SiO_4 spinel solid solutions. Earth and Planetary Science Letters, 1966, 1(4), 241-245.

Ringwood, A.E., and Major, A. (1967) High-pressure reconnaissance investigations in the system Mg_2SiO_4-MgO-H_2O. Earth and Planetary Science Letters, 2, 2, 130-133.

Rivers, M., Prakapenka, V.B., Kubo, A., Pullins, C., Holl, C.M., Jacobsen, S.D. (2008) The COMPRES/GSECARS gas-loading system for diamond anvil cells at the Advanced Photon Source. High Pressure Res 28(3), 273-292.

Rubie, D.C. (1999) Characterising the sample environment in multianvil high-pressure experiments. Phase Transitions, 68(3), 431-451.

Sheldrick, G.M. (2018) SHELXL: Programs for crystal structure analysis. University of Göttingen, Germany.

Shieh, S. R., Mao, H. K., Hemley, R. J., and Ming, L. C. (2000) In situ X-ray diffraction studies of dense hydrous magnesium silicates at mantle conditions. Earth and Planetary Science Letters, 177, 1-2, 69-80.

Shieh, S. R., Duffy, T. S., Liu, Z., and Ohtani, E. (2009) High-pressure infrared spectroscopy of the dense hydrous magnesium silicates phase D and phase E.

Physics of the Earth and Planetary Interiors, 175, 106-114.

Takahashi, E. (1986) Melting of a dry peridotite KLB-1 up to 14 GPa: Implications on the origin of peridotitic upper mantle. Journal of Geophysical Research-Solid Earth and Planets, 91, B9, 9367-9382.

Tomioka, N., Okuchi, T., Purevjav, N., Abe, J., and Harjo, S. (2016) Hydrogen sites in the dense hydrous magnesian silicate phase E: a pulsed neutron powder diffraction study. Physics and Chemistry of Minerals, 43(4), 267-275.

Uchiyama H., Kuribayashi, T., and Kudoh, Y. (2011) Estimation of hydrous position in (Fe, Al)-bearing phase E structure using single-crystal diffraction data. Photon Factory Activity Report.

FIGURE CAPTIONS

Figure 1. Polyhedral representation of phase E (modified after Tomioka et al. 2016).

Figure 2. Backscattered electron (BSE) images of coexisting phases. (a) run SS1601 contains ringwoodite, phase E, garnet, and phase δ-H. (b) run SS1603 contains wadsleyite, phase E, garnet, clinoenstatite, and phase δ-H. Abbreviations: Wd = wadsleyite, Rw = ringwoodite, Cen = clinoenstatite, PhE =phase E, Gt =garnet, Phδ-H = phase δ-H.

Figure 3. Raman and fluorescence bands (labeled in cm^{-1} and nm respectively) of phase E. **(a)** at ambient conditions excited at 532 nm. Raman bands were confirmed by excitation at 532 nm. **(b)** at ambient conditions excited at 514.5 nm. Raman bands were confirmed by excitation at 488 nm (Kleppe et al. 2001).

Figure 4. Representative Raman spectra at ambient conditions. **(a)** two Fe-bearing phase E samples (from run products of SS1601 and SS1603, respectively) in this study and pure-Mg phase E reported by Kleppe et al. (2001). The relative intensities of the bands vary with changing orientation of the phase E crystals (SS1601 and SS1603) relative to the incident beam, and this does not indicate different modes. **(b)** wadsleyite (from run products of SS1603) and ringwoodite (from run products of SS1601) in this study.

Figure 5. (a) Representative Raman spectra of phase E under compression to 19 GPa. (**b)** The frequency shifts of framework Raman modes as a function of pressure for phase E. Errors in measurement of both frequency and pressure are within the size of the symbols.

Figure 6. The correlation between site occupancies and Fe/Mg molar ratios. Some error bars are within the size of the symbols.

Appendix Figure 1. Precession images for axial crystallographic directions (0kl, h0l, and hk0) of two phase E samples.

Table 1. Representative chemical compositions of minerals

Oxide (wt%)	SS1601 PhE	SS1601 Rw	SS1601 Gt	SS1601 Phδ-H	SS1603 PhE	SS1603 Wd	SS1603 Cpx	SS1603 Gt	SS1603 Phδ-H
SiO_2	37.93	39.11	40.67	6.32	37.56	43.35	57.92	39.69	4.66
MgO	43.07	37.90	11.80	3.67	44.76	50.04	39.80	24.50	3.08
FeO	6.18	21.39	15.31	2.60	4.47	3.23	1.24	16.82	5.65
Al_2O_3	1.48	0.02	22.74	68.71	1.41	0.03	0.10	0.71	68.66
CaO	0.08	0.00	9.27	0.30	0.06	0.05	0.12	16.51	0.02
TiO_2	0.04	0.00	0.15	0.58	0.04	0.10	0.00	0.20	0.55
Total	88.78	98.42	99.94	82.18	88.30	96.80	99.18	98.43	82.62

Abbreviations: PhE = Phase E, Rw = ringwoodite, Gt = garnet, Phδ-H = Phase δ-H, Wd = wadsleyite, and Cpx = clinopyroxene.

Table 2. Positional parameters and selected bond distances for the two samples of phase E

	Sample 1	Sample 2
	M1	
Occupancy	0.752(10)	0.721(7)
z	0.000	0.000
<M1-O>	2.0764(17)	2.0702(12)
	M2	
Occupancy	0.024	0.029
z	0.500	0.500
<M2-O>	2.0690(17)	2.0609(12)
	Si	
Occupancy	0.189(6)	0.198(4)
z	0.1292(4)	0.1293(2)
<Si-O>	1.832(2)	1.8238(13)
<Si-O>	1.670(6)	1.666(3)

According to the electron microprobe analyses, the formula units of sample 1 and sample 2 were estimated to be $Mg_{2.08}Fe_{0.17}Al_{0.06}Si_{1.23}O_6H_{2.43}$ and $Mg_{2.15}Fe_{0.10}Al_{0.03}Si_{1.26}O_6H_{2.39}$, respectively. All atoms in atomic positions 0, 0, *z* in the average structure based on a hexagonal unit cell with space group *R*-3*m*. Unit-cell parameters are a = 2.9787(5), c = 13.883(3) and a = 2.9650(13), c = 13.870(4) for two samples, respectively. Si site has one short Si-O bond and three long Si-O bonds.

Figure 1

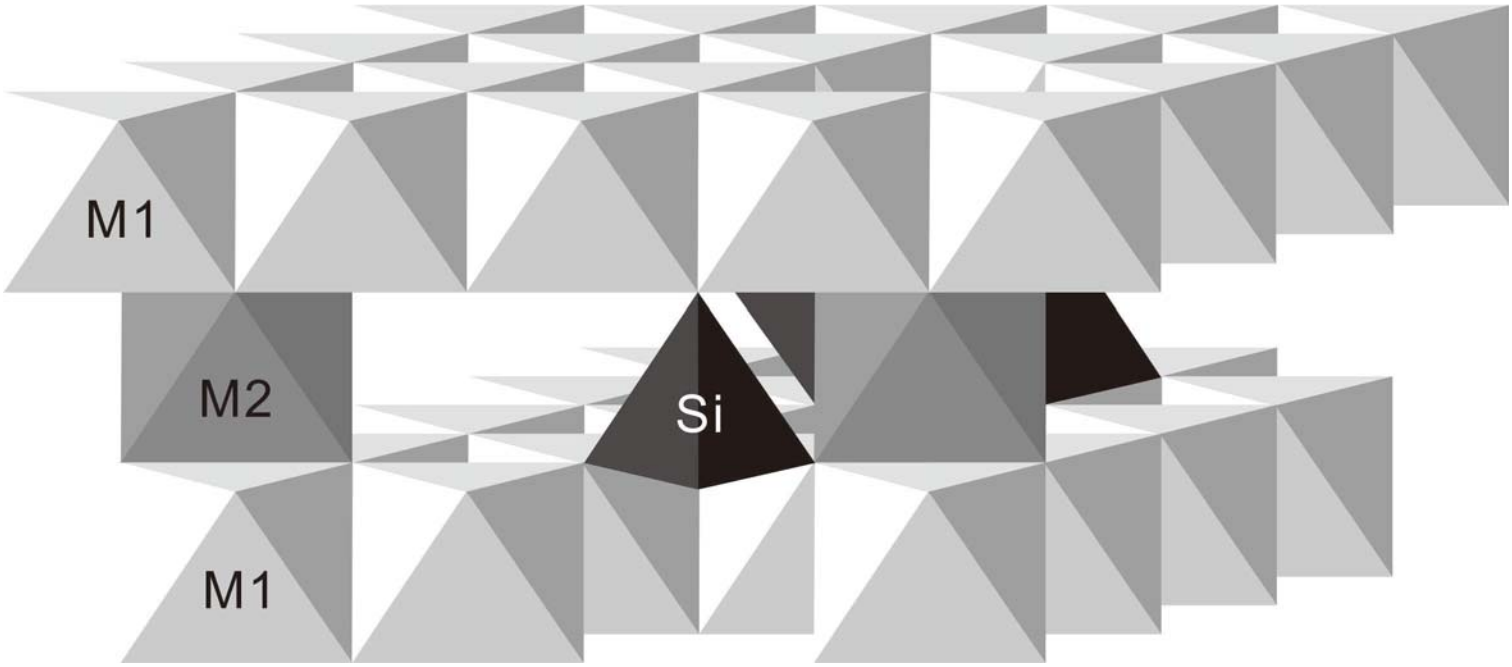

Figure 2

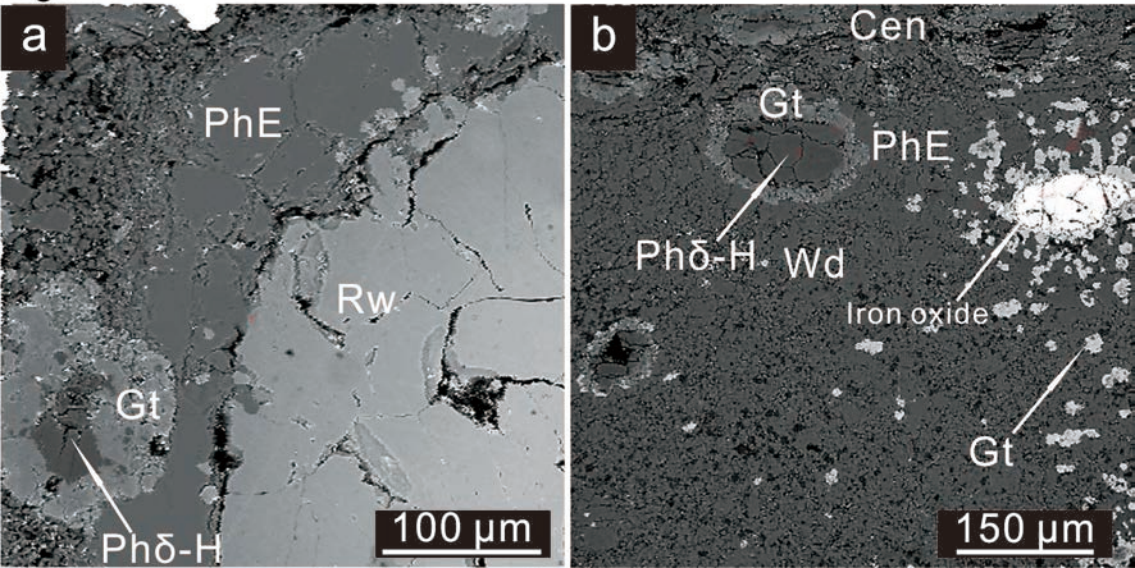

Figure 3

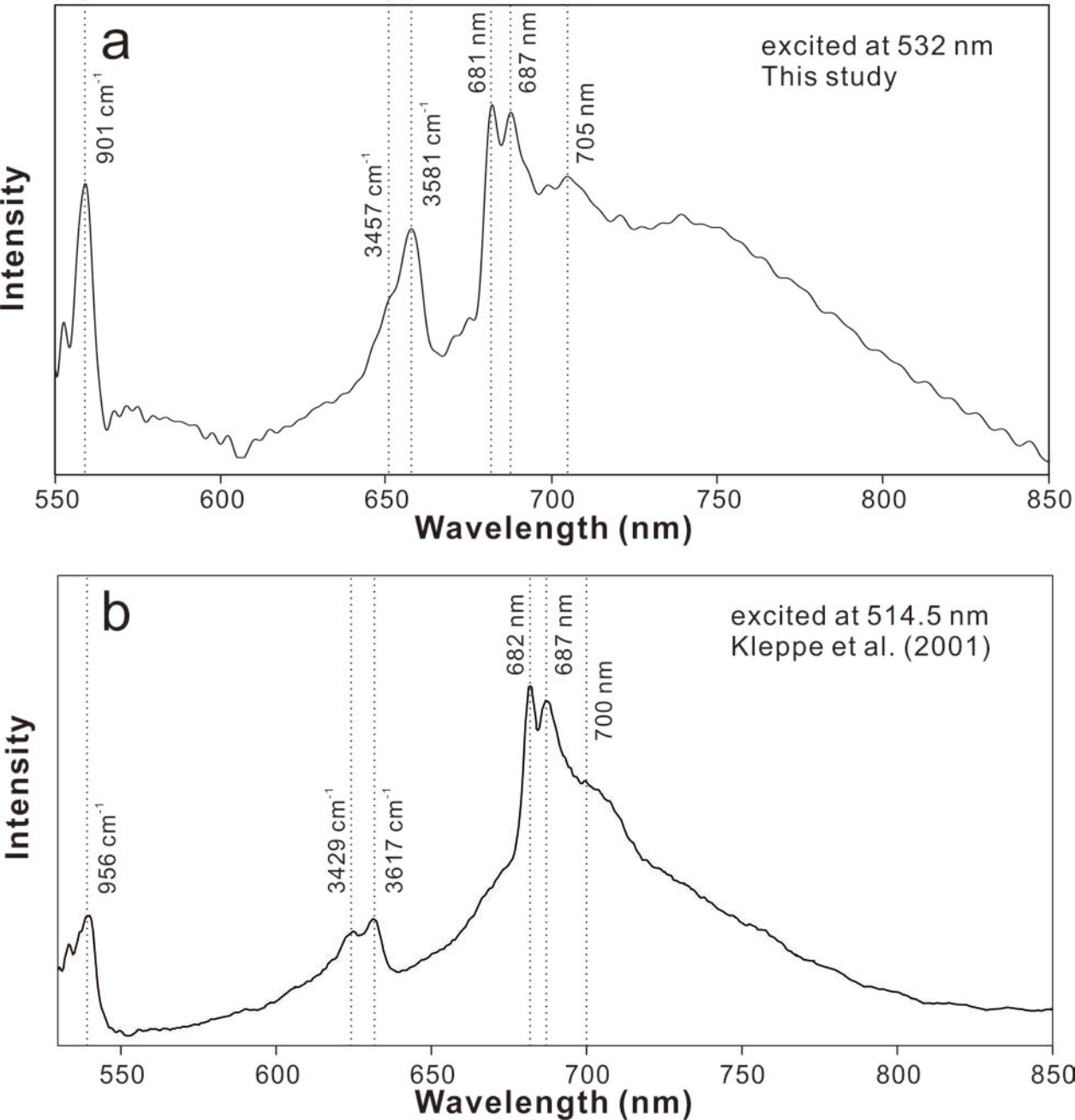
a
excited at 532 nm
This study
901 cm-1
3457 cm-1
3581 cm-1
681 nm
687 nm
705 nm
Intensity
550
600
650
700
750
800
850
Wavelength (nm)
b
excited at 514.5 nm
Kleppe et al. (2001)
956 cm-1
3429 cm-1
3617 cm-1
682 nm
687 nm
700 nm
Intensity
550
600
650
700
750
800
850
Wavelength (nm)

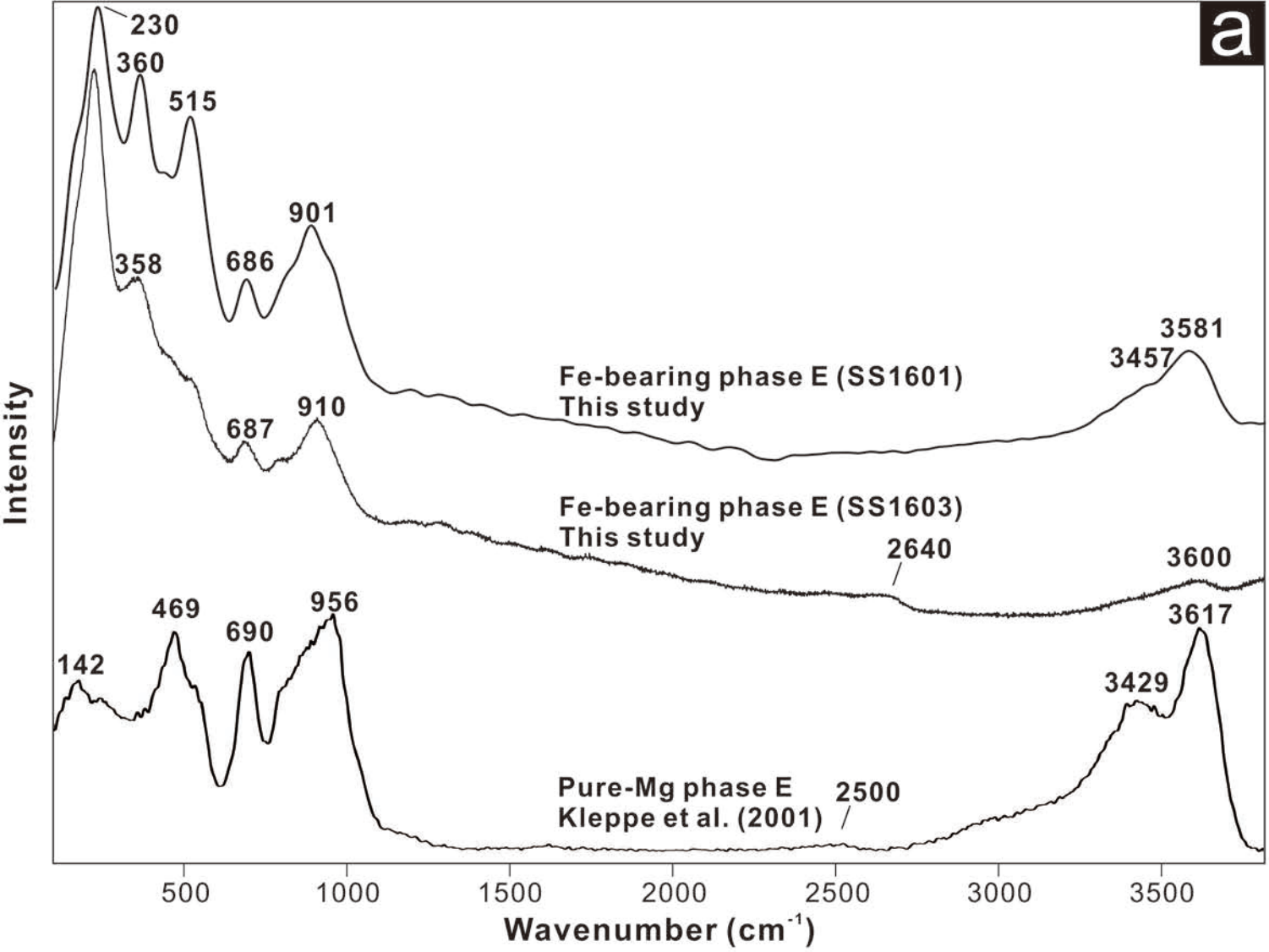
a
230
360
515
901
358
686
3581
3457
Fe-bearing phase E (SS1601)
This study
687
910
Fe-bearing phase E (SS1603)
This study
2640
3600
469
956
690
3617
142
3429
Pure-Mg phase E
Kleppe et al. (2001)
2500
Intensity
500
1000
1500
2000
2500
3000
3500
Wavenumber (cm-1)

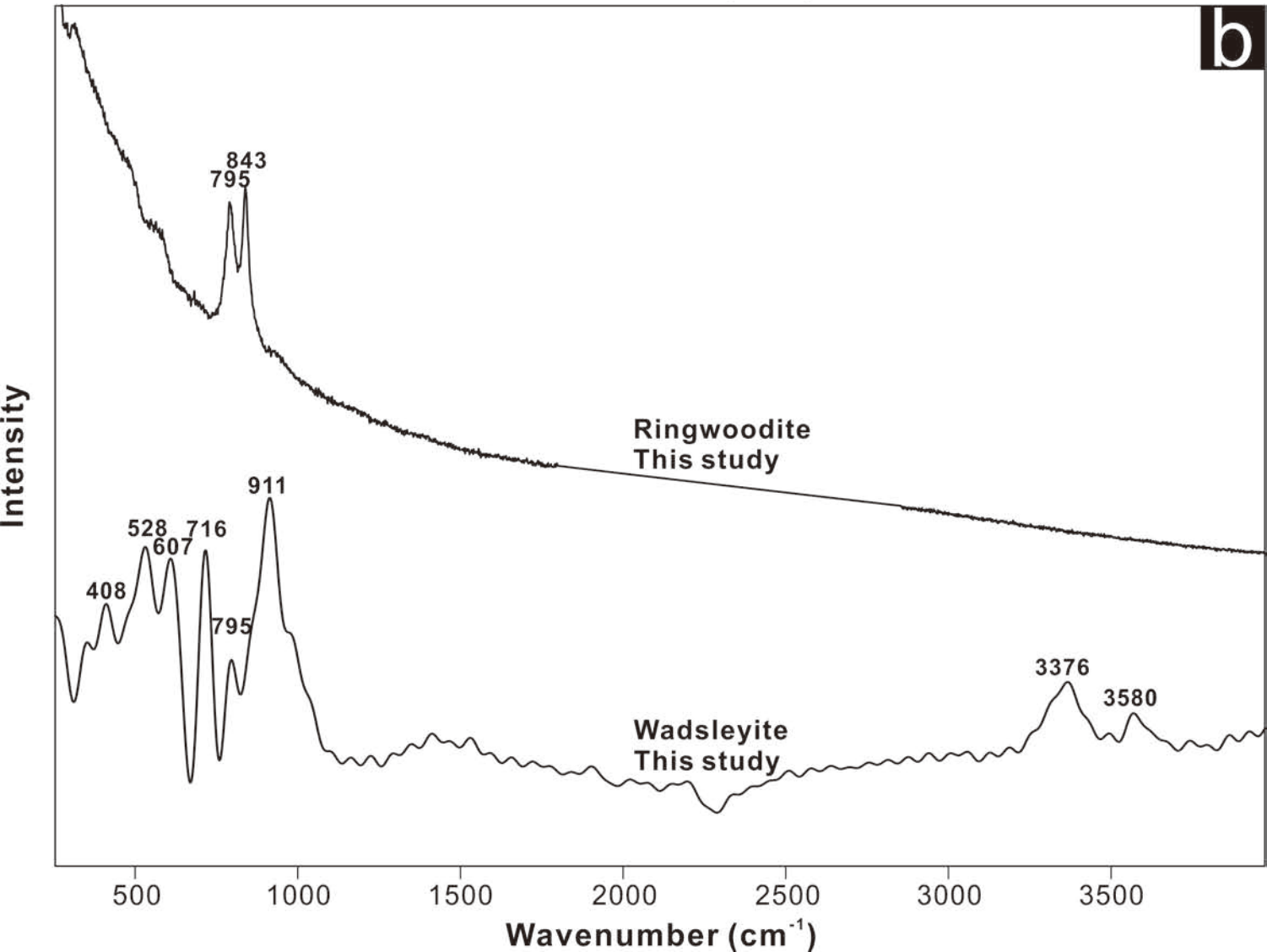
b
843
795
Ringwoodite
This study
911
528
716
607
408
795
3376
3580
Wadsleyite
This study
Intensity
500
1000
1500
2000
2500
3000
3500
Wavenumber (cm-1)

Figure 5

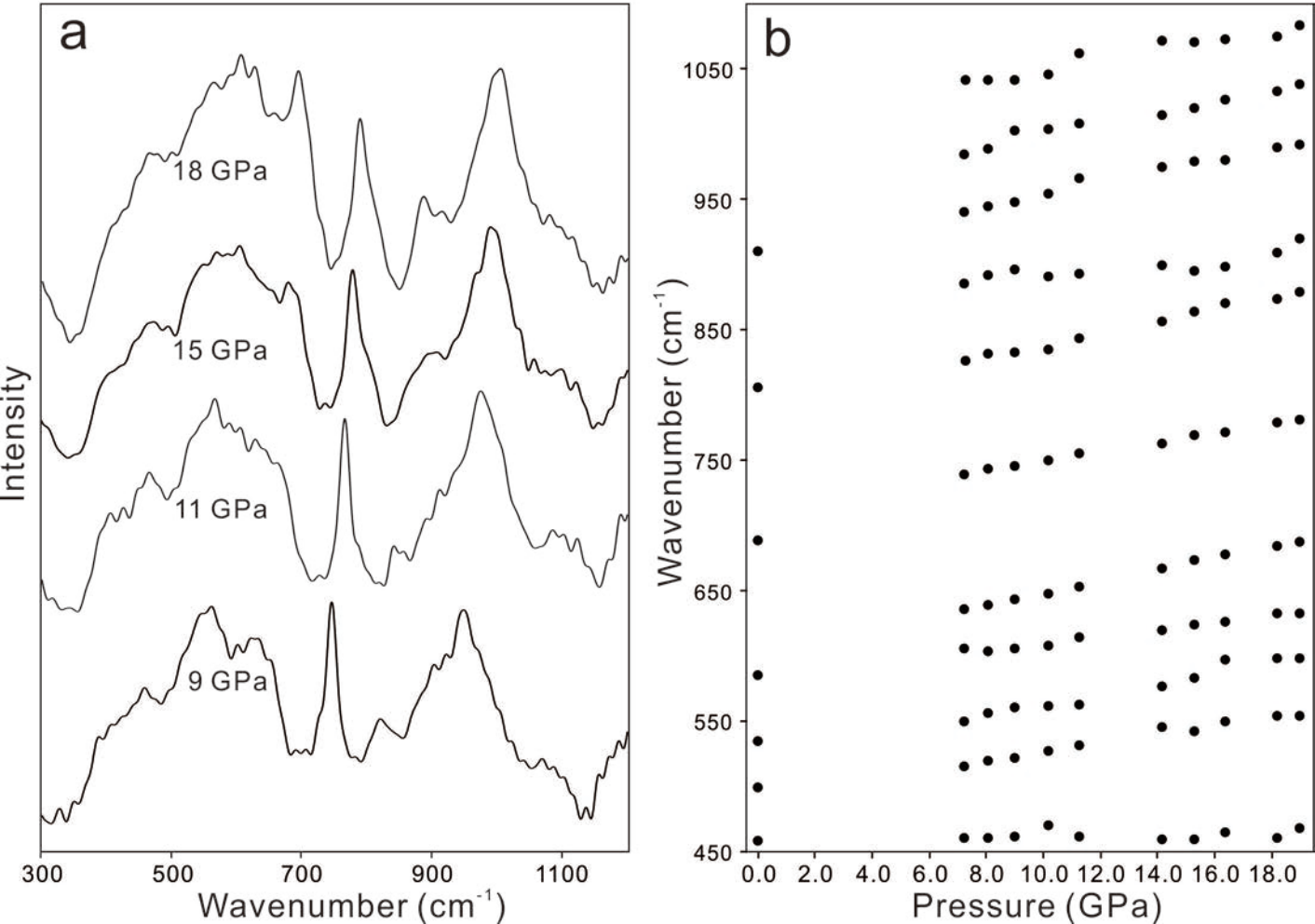
a
18 GPa
15 GPa
11 GPa
9 GPa
Intensity
300
500
700
900
1100
Wavenumber (cm-1)
b
1050
950
850
750
650
550
450
Wavenumber (cm-1)
0.0
2.0
4.0
6.0
8.0
10.0
12.0
14.0
16.0
18.0
Pressure (GPa)

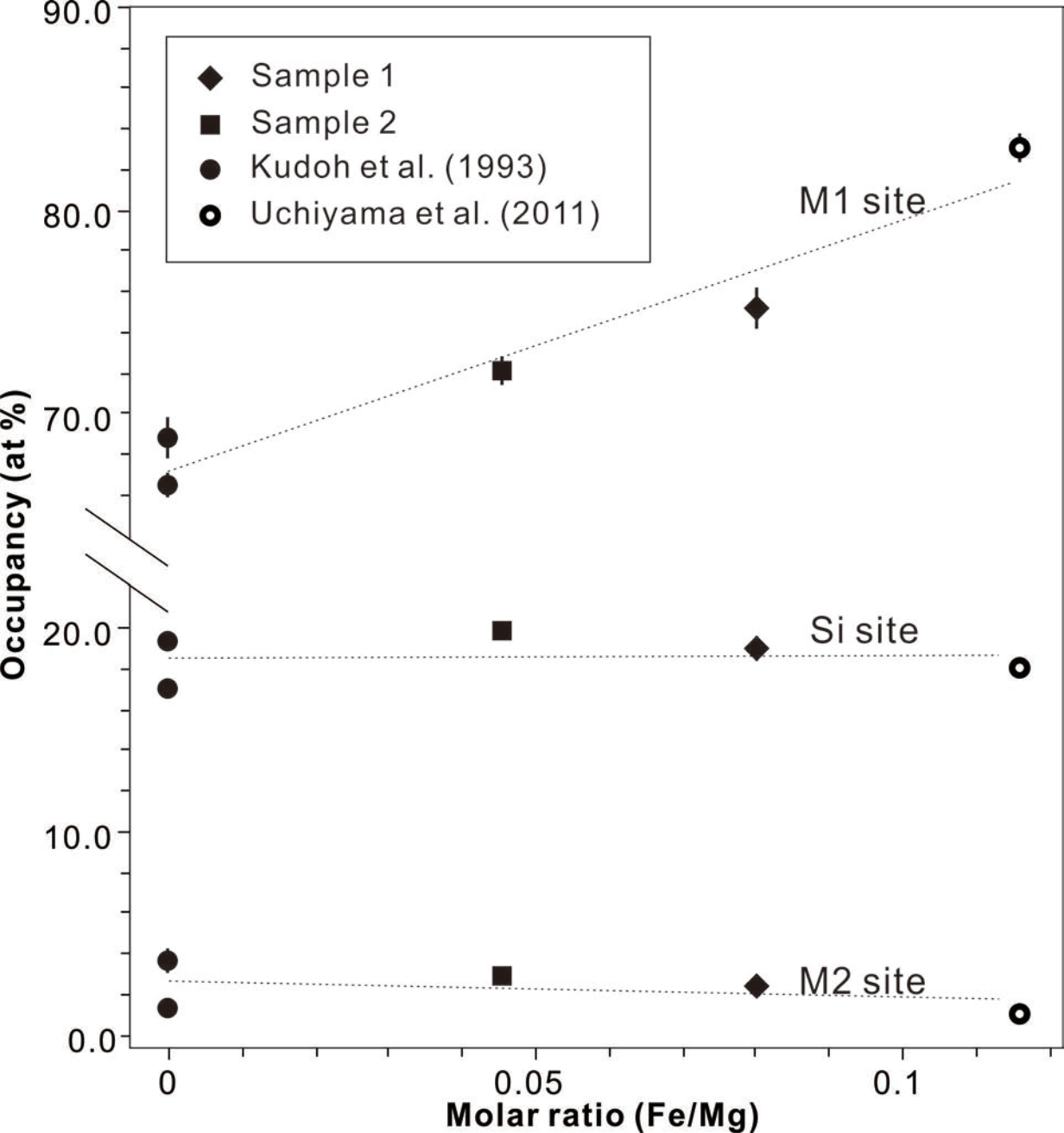
Sample 1
Sample 2
Kudoh et al. (1993)
Uchiyama et al. (2011)
M1 site
Si site
M2 site
Occupancy (at %)
Molar ratio (Fe/Mg)
90.0
80.0
70.0
20.0
10.0
0.0
0
0.05
0.1